

Probabilistic quantum teleportation via thermal entanglement

Raphael Fortes¹ and Gustavo Rigolin^{2,*}

¹*Universidade Federal da Integração Latino Americana, 85867-970, Foz do Iguaçu, PR, Brazil*

²*Departamento de Física, Universidade Federal de São Carlos, 13565-905, São Carlos, SP, Brazil*

(Dated: December 3, 2024)

We study the probabilistic (conditional) teleportation protocol when the entanglement needed to its implementation is given by thermal entanglement, i.e., when the quantum channel connecting Alice and Bob is an entangled mixed state described by the canonical ensemble density matrix. Specifically, the quantum channel we employ here is given by two interacting spin-1/2 systems (two qubits) in equilibrium with a thermal reservoir at temperature T . The interaction between the qubits is described by a Heisenberg-like Hamiltonian, encompassing the Ising, the XX, the XY, the XXX, and XXZ models, with or without external fields. For all those models we show analytically that the probabilistic protocol is exactly equal to the deterministic one whenever we have no external field. However, when we turn on the field the probabilistic protocol outperforms the deterministic one in several interesting ways. Under certain scenarios, for example, the efficiency of the probabilistic protocol is greater than the deterministic one and increases with increasing temperature, a counterintuitive behavior. We also show regimes in which the probabilistic protocol operates with relatively high success rates and, at the same time, with efficiency greater than the classical limit 2/3, above which a genuine quantum teleportation takes place. The deterministic protocol's efficiency under the same conditions is below 2/3, highlighting that the probabilistic protocol is the only one yielding a genuine quantum teleportation. We also show that near the quantum critical points for almost all those models the qualitative and quantitative behaviors of the efficiency change considerably, even at finite T .

PACS numbers: 03.65.Ud, 03.67.Bg, 03.67.Hk

I. INTRODUCTION

The quantum teleportation protocol [1] is one of the most important quantum communication protocols devised so far. It was originally built [1] to transfer an unknown quantum state $|\psi\rangle$, describing a qubit located in one place (Alice's), to another qubit in another place (Bob's) without sending the physical system originally described by $|\psi\rangle$ from Alice to Bob. A few years after its conception, the teleportation protocol was extended to continuous variable systems [2, 3] and also the first experimental realizations were presented [4–6]. The key resource needed to accomplish such a task without corrupting the teleported state is a maximally entangled pure state that Alice and Bob must share. This maximally entangled pure state is the ideal quantum channel through which the teleportation takes place.

Generating and preserving a maximally entangled pure state is not easy. Unavoidable losses, noise, and decoherence rapidly reduce its purity and entanglement. A workaround to bypass those problems using only local operations and classical communication is entanglement distillation [7], where several copies of non-maximally entangled mixed states are converted into one maximally entangled pure state. A different approach is based on the modification of the standard teleportation protocols [1–3], adapting them to operate directly with non-

maximally entangled states [8–21].

The modified teleportation protocols can be divided into two main groups. The first one contains the deterministic protocols [11–22], in which there is no postselection of the measurement results obtained by Alice during the execution of the protocol. In other words, at the end of each run of the protocol, no matter what measurement outcome Alice obtains, Bob considers his qubit as a valid output of the teleportation protocol. The word “deterministic” means that the probability of “success” is one for those protocols, even if Bob's qubit at the end of the protocol is not exactly equal to the input state. The second group contains the probabilistic protocols, in which Alice and Bob postselect certain measurement results of Alice. In this scenario, Alice's measurement outcomes leading to low fidelity teleported states are discarded and thus the protocol is dubbed probabilistic since the chances of Alice getting the measurement results leading to high fidelity teleported states are less than one [8–10, 23].

Most of the works dealing with probabilistic teleportation protocols employ non-maximally pure entangled states as the quantum channel connecting Alice and Bob [8–10]. Only recently was presented a comprehensive investigation of the probabilistic protocol with mixed entangled states [23]. In Ref. [23] each qubit of a maximally entangled pure state (Bell state) was independently subjected to all possible combinations of the four standard types of noise one faces in the implementation of quantum communication tasks, namely, the bit flip, the phase flip or phase dumping, the depolarizing, and the amplitude damping noise channels. The efficiency to teleport

*Electronic address: rigolin@ufscar.br

a qubit of each one of the 16 mixed states obtained after the action of those kinds of noise was studied. It was also assumed that Alice's qubit might also be acted by each one of those four types of noise, giving a total of 64 case studies.

In this manuscript our goal is to study a different yet important noise scenario. We now consider that the two qubits shared between Alice and Bob can interact and that they are in thermal equilibrium with a thermal reservoir at temperature T (see Fig. 1). This scenario naturally appears in a possible implementation of a quantum computer based on solid state devices, where quantum information needs to be transferred (teleported) from one location to another inside a quantum chip and T is the temperature under which the quantum computer operates.

The quantum state of a two-qubit system in equilibrium with a thermal reservoir is described by the canonical ensemble density matrix and whenever entanglement is present between the two qubits it is usually called *thermal entanglement* [24–32]. In this manuscript we model the interaction between the qubits of the quantum channel via the Heisenberg Hamiltonian, either without or with an external magnetic field. The external magnetic field gives an important extra control parameter that can be tuned to maximize the teleportation efficiency. For several combinations of the coupling constants and external field in the Heisenberg Hamiltonian, we obtain counter-intuitive situations where an increase of the temperature leads to a better teleportation. Also, we show that there are cases where the probabilistic protocol beats the deterministic one in a very important way, already seen in the noise models of Ref. [23]: we prove that for some set of coupling constants in the Heisenberg model, the probabilistic protocol is the only one leading to a genuine quantum teleportation. This is true because the deterministic protocol under the same conditions cannot overcome the efficiency (average fidelity) of an all-classical protocol, where no entanglement is used to teleport the qubit. The probabilistic protocol, on the other hand, has an efficiency that cannot be achieved by the all-classical protocol. We also investigate how the efficiencies of the probabilistic and deterministic protocols are affected in the vicinity of the quantum critical points for the models we study here. We noted non-trivial qualitative and quantitative changes in the behavior of the efficiencies near the critical points, even at finite T .

II. THE MATHEMATICAL TOOLS

Since the quantum channel in the present manuscript is not a pure state, we have to recast the original teleportation protocol using the language of density matrices. This was done for the deterministic protocol in Ref. [20] and for the probabilistic protocol in Ref. [23]. In Secs. II A and II B we review the main ideas and results of those references that are needed here. We follow closely the no-

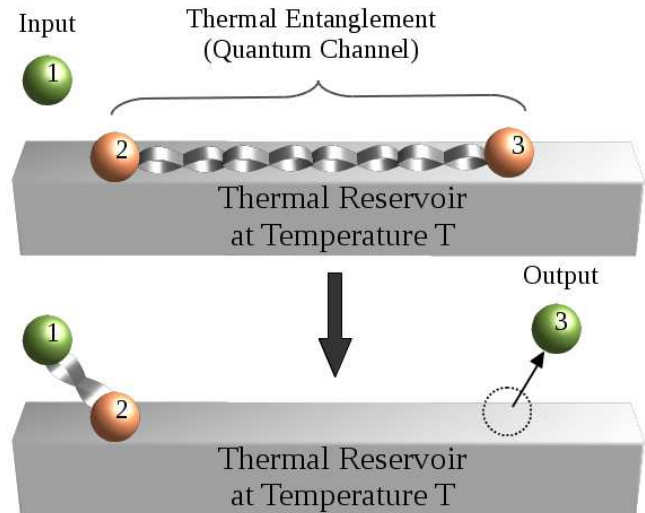


FIG. 1: (color online) The teleportation protocol can basically be divided into four steps. Upper panel: The first step is related to the preparation of the quantum channel (qubits 2 and 3) and the input (qubit 1). Here the quantum channel is described by two interacting qubits in thermal equilibrium with a thermal reservoir at temperature T . Lower panel: The second step consists in Alice implementing a joint measurement (Bell measurement) in the input and her share of the quantum channel (qubits 1 and 2), which become entangled. Step three is the broadcasting to Bob, via a classical communication channel, of Alice's measurement result. In the fourth and last step, Bob implements a unitary operation on the output state (qubit 3) depending on the result of Alice's measurement. Note that the present analysis is particularly relevant and meaningful whenever the overall time needed to implement all steps of the teleportation protocol is lower than the time needed by the whole system to be brought back to thermal equilibrium. In other words, the rate at which we implement all steps of the teleportation protocol must be higher than the system's thermal relaxation rate. In the opposite scenario, however, Bob's output qubit would return to a thermal equilibrium state before we could access and further manipulate its content or even before we could finish the teleportation protocol. In this case the present analysis does not apply.

tation and style of Refs. [20, 23]. In Sec. II C we present the Heisenberg model, preparing the ground for Sec. III, where we show the main results of this manuscript.

A. Recasting the teleportation protocol in the density matrix formalism

The input qubit that is teleported from Alice to Bob is assumed a pure state and is given by $|\psi\rangle_{in} = a|0\rangle + b|1\rangle$, with $|a|^2 + |b|^2 = 1$. Its density matrix is

$$\rho_{in} = |\psi\rangle_{in} \langle \psi| = \begin{pmatrix} |a|^2 & ab^* \\ a^*b & |b|^2 \end{pmatrix}, \quad (1)$$

where $*$ is complex conjugation and the subscript *in* means “input”. The entangled state shared between Al-

ice and Bob (the quantum channel) is described by the canonical ensemble density matrix,

$$\rho_{ch} = \frac{e^{-\frac{H}{kT}}}{Z} = \frac{e^{-\beta H}}{Z}, \quad (2)$$

where $Z = \text{Tr}(e^{-H/kT})$ is the partition function, “Tr” is the trace operation, k is the Boltzmann constant, and ch means “channel”. The Hamiltonian H is given by the Heisenberg model as explained in Sec. II C.

At this stage, the total state describing all qubits is

$$\rho = \rho_{in} \otimes \rho_{ch}. \quad (3)$$

The teleportation protocol proceeds as follows:

- (i) Alice implements a Bell state measurement onto qubits 1 and 2.
- (ii) Alice broadcasts her measurement result to Bob using a classical communication channel.
- (iii) Bob uses the information received in step (ii) to choose the right unitary operation to be applied on his state (qubit 3).

If Alice and Bob shared a maximally entangled pure state (Bell state), at the end of step (iii) Bob’s qubit would be exactly described by ρ_{in} . In any realistic scenario this is not the case and we invariably have a mixed state describing the quantum channel, leading to a non-perfect teleportation.

The projectors describing Alice’s measurement on the input qubit and her qubit of the quantum channel are

$$P_j^\varphi = |B_j^\varphi\rangle\langle B_j^\varphi|, \quad j = 1, 2, 3, 4, \quad (4)$$

with

$$|B_1^\varphi\rangle = \cos \varphi |00\rangle + \sin \varphi |11\rangle, \quad (5)$$

$$|B_2^\varphi\rangle = \sin \varphi |00\rangle - \cos \varphi |11\rangle, \quad (6)$$

$$|B_3^\varphi\rangle = \cos \varphi |01\rangle + \sin \varphi |10\rangle, \quad (7)$$

$$|B_4^\varphi\rangle = \sin \varphi |01\rangle - \cos \varphi |10\rangle. \quad (8)$$

In the standard protocol $\varphi = \pi/4$ and $|B_j\rangle$, $j = 1, 2, 3, 4$, are respectively the Bell states $|\Phi^+\rangle$, $|\Phi^-\rangle$, $|\Psi^+\rangle$, and $|\Psi^-\rangle$ [1]. Here φ is a free parameter chosen by Alice to maximize the efficiency of the probabilistic teleportation.

Alice’s probability to measure a given generalized Bell state is

$$Q_j(|\psi\rangle_{in}) = \text{Tr}[P_j^\varphi \rho] \quad (9)$$

and at the end of step (iii) Bob’s state is

$$\rho_{B_j} = \frac{U_j \text{Tr}_{12}[P_j^\varphi \rho P_j^\varphi] U_j^\dagger}{Q_j(|\psi\rangle_{in})}. \quad (10)$$

Here Tr_{12} is the partial trace on the first two qubits (Alice’s qubits). We make it explicit the dependence of Q_j

on the input state $|\psi\rangle_{in}$ since for mixed state channels, or non-maximally entangled channels, the probability depends on the input state [8–10, 20, 23].

In the standard teleportation protocol the unitary transformation that Bob implements on his qubit depends not only on Alice’s measurement outcome but also on the quantum channel [1]. For example, if ρ_{ch} is the Bell state $|\Phi^+\rangle = (|00\rangle + |11\rangle)/\sqrt{2}$ we have $U_1 = \mathbb{1}$, $U_2 = \sigma_z$, $U_3 = \sigma_x$, and $U_4 = \sigma_z \sigma_x$, with $\mathbb{1}$ being the identity matrix and σ_z and σ_x the standard Pauli matrices. For the other three Bell states, $|\Phi^-\rangle$, $|\Psi^+\rangle$, and $|\Psi^-\rangle$, we have respectively $\{U_1, U_2, U_3, U_4\} = \{\sigma_z, \mathbb{1}, \sigma_z \sigma_x, \sigma_x\}$, $\{\sigma_x, \sigma_z \sigma_x, \mathbb{1}, \sigma_z\}$, and $\{\sigma_z \sigma_x, \sigma_x, \sigma_z, \mathbb{1}\}$. With that in mind, when we search for the optimal settings leading to the greatest efficiency for the teleportation protocol, we will also let U_j run over its possible four values: $\mathbb{1}, \sigma_z, \sigma_x, \sigma_z \sigma_x$.

B. Success rate and efficiency of the probabilistic teleportation

Since the chance Q_j of Alice measuring the generalized Bell state $|B_j^\varphi\rangle$ when she shares with Bob a non-maximally entangled channel depends on the input state $|\psi\rangle_{in}$ [8–10, 20, 23], we assume $|\psi\rangle_{in}$ is given by a uniform probability distribution (Haar measure),

$$P_X(x) = \mathcal{P}(|\psi\rangle_{in}). \quad (11)$$

Here X denotes a continuous random variable whose values x are all possible pure qubits that together define the sample space Ω . Averaging over this distribution we obtain input-state-independent results for the relevant quantities needed to study the efficiency of the teleportation protocol. The probability distribution $P_X(x)$ is normalized as follows,

$$\int_{\Omega} P_X(x) dx = \int_{\Omega} \mathcal{P}(|\psi\rangle_{in}) d|\psi\rangle_{in} = 1, \quad (12)$$

where $P_X(x)$ is constant for all x .

If we write an arbitrary qubit as

$$|\psi\rangle = \alpha |0\rangle + \delta e^{i\gamma} |1\rangle, \quad (13)$$

where $\alpha \geq 0$, $\delta \geq 0$, $\alpha^2 + \delta^2 = 1$, and $0 \leq \gamma \leq 2\pi$ are real numbers, it is not difficult to see that we can select α^2 and γ as independent variables. Thus $\mathcal{P}(|\psi\rangle_{in}) = \mathcal{P}(\alpha^2, \gamma)$ and Eq. (12) reads

$$\int_0^{2\pi} \int_0^1 \mathcal{P}(\alpha^2, \gamma) d\alpha^2 d\gamma = 1, \quad (14)$$

where

$$\mathcal{P}(\alpha^2, \gamma) = \frac{1}{2\pi} \quad (15)$$

for a uniform distribution.

There is also a discrete variable J with values $j = 1, 2, 3, 4$ (or $j = \Phi^+, \Phi^-, \Psi^+, \Psi^-$) representing the generalized Bell states $|B_j^\varphi\rangle$. Thus, the probability to measure $|B_j^\varphi\rangle$ is denoted by $P_J(j)$. The conditional probability $P_{J|X}(j|x)$ gives Alice's chance of measuring the Bell state j if the input state to be teleported is x and is given by Eq. (9),

$$P_{J|X}(j|x) = Q_j(|\psi\rangle_{in}). \quad (16)$$

The joint probability distribution $P_{XJ}(x, j) = P_{JX}(j, x)$ can be obtained if we use the definition of the conditional probability,

$$P_{XJ}(x, j) = P_X(x)P_{J|X}(j|x) = \mathcal{P}(|\psi\rangle_{in})Q_j(|\psi\rangle_{in}), \quad (17)$$

which subsequently allows us to compute the marginal distribution $P_J(j) = \int_{\Omega} P_{XJ}(x, j)dx$,

$$P_J(j) = \int_{\Omega} \mathcal{P}(|\psi\rangle_{in})Q_j(|\psi\rangle_{in})d|\psi\rangle_{in}. \quad (18)$$

And if we use Eq. (17) exchanging the roles of X with J and Eq. (18) we arrive at

$$\begin{aligned} P_{X|J}(x|j) &= \frac{P_{XJ}(x, j)}{P_J(j)} \\ &= \frac{\mathcal{P}(|\psi\rangle_{in})Q_j(|\psi\rangle_{in})}{\int_{\Omega} \mathcal{P}(|\psi\rangle_{in})Q_j(|\psi\rangle_{in})d|\psi\rangle_{in}}. \end{aligned} \quad (19)$$

These last two expressions, Eqs. (18) and (19), are the probability distributions needed to quantitatively study the probabilistic teleportation protocol.

We can better appreciate the last statement remembering the meaning of $P_J(j)$ and $P_{X|J}(x|j)$. Noting that $P_J(j)$ gives the chance of Alice measuring the generalized Bell state $|B_j^\varphi\rangle$ when the distribution for the input states is $\mathcal{P}(|\psi\rangle_{in})$, it is straightforward to see that $P_J(j)$ is the average probability of measuring $|B_j^\varphi\rangle$,

$$\overline{Q}_j = P_J(j) = \int_{\Omega} \mathcal{P}(|\psi\rangle_{in})Q_j(|\psi\rangle_{in})d|\psi\rangle_{in}. \quad (20)$$

\overline{Q}_j does not depend on $|\psi\rangle_{in}$ and is called the probability of success or the success rate of the probabilistic teleportation protocol if we postselect the measurement result j [23].

To quantify how similar to the input state is the output after one run of the protocol we employ the fidelity [36], which for a pure input state is

$$F_j(|\psi\rangle_{in}) = \text{Tr}[\rho_{in}\rho_{B_j}] = {}_{in}\langle\psi|\rho_{B_j}|\psi\rangle_{in}, \quad (21)$$

with ρ_{B_j} , Eq. (10), being the output state with Bob after the teleportation protocol ends. For a perfect teleportation $F_j = 1$ (its maximal value) and $F_j = 0$ (its minimal value) when the output is orthogonal to the input state.

Looking at Eq. (21) we see that in general F_j depends on $|\psi\rangle_{in}$ and by averaging over all possible input states

we get an input-state-independent quantification for the efficiency of the protocol [23]. Since we are interested in a postselected measurement result j , the distribution of input states $|\psi\rangle_{in}$ in this situation is $P_{X|J}(x|j)$, Eq. (19), which leads to the following average fidelity,

$$\begin{aligned} \overline{F}_j &= \int_{\Omega} F_j(x)P_{X|J}(x|j)dx \\ &= \frac{\int_{\Omega} F_j(|\psi\rangle_{in})\mathcal{P}(|\psi\rangle_{in})Q_j(|\psi\rangle_{in})d|\psi\rangle_{in}}{\int_{\Omega} \mathcal{P}(|\psi\rangle_{in})Q_j(|\psi\rangle_{in})d|\psi\rangle_{in}}. \end{aligned} \quad (22)$$

This is what we call the efficiency of the probabilistic teleportation protocol if we postselect the measurement result j [23]. If all measurement results are accepted, i.e., no postselection is made, we get back the efficiency of the deterministic protocol [20, 23],

$$\langle \overline{F} \rangle = \sum_{j=1}^4 P_J(j)\overline{F}_j = \int_{\Omega} \overline{F}(|\psi\rangle_{in})\mathcal{P}(|\psi\rangle_{in})d|\psi\rangle_{in}, \quad (23)$$

$$\text{where } \overline{F}(|\psi\rangle_{in}) = \sum_j^4 Q_j(|\psi\rangle_{in})F_j(|\psi\rangle_{in}).$$

Following the strategy of Ref. [23], we want to maximize Eq. (22) over the set of free parameters present in the probabilistic protocol. In particular, we want to get scenarios in which $\overline{F}_j > \langle \overline{F} \rangle$, where $\langle \overline{F} \rangle$ is the optimal efficiency of the deterministic teleportation protocol.

C. The Heisenberg model

The Hamiltonian describing the Heisenberg model for a spin-1/2 chain of two qubits is

$$H = j_x\sigma_x^{(2)}\sigma_x^{(3)} + j_y\sigma_y^{(2)}\sigma_y^{(3)} + j_z\sigma_z^{(2)}\sigma_z^{(3)} + h_a\sigma_z^{(2)} + h_b\sigma_z^{(3)}, \quad (24)$$

where $\sigma_j^{(2)}\sigma_j^{(3)} = \sigma_j^{(2)} \otimes \sigma_j^{(3)}$, with the superscripts (2) and (3) representing qubits 2 (with Alice) and 3 (with Bob) of the quantum channel (see Fig. 1). In Eq. (24), σ_j , $j = x, y, z$, are the standard Pauli matrices such that $\sigma_z|0\rangle = |0\rangle$ and $\sigma_z|1\rangle = -|1\rangle$, $\sigma_x|0\rangle = |1\rangle$ and $\sigma_x|1\rangle = |0\rangle$, and $\sigma_y|0\rangle = i|1\rangle$ and $\sigma_y|1\rangle = -i|0\rangle$, with i being the imaginary unity. Furthermore, j_x, j_y, j_z, h_a, h_b are real numbers with the former three representing the coupling constants between the qubits and the latter two denoting external magnetic fields applied respectively on qubits 2 and 3 along the z direction.

Inserting Eq. (24) into Eq. (2) we get the canonical ensemble density matrix describing the quantum channel ρ_{ch} , which together with Eq. (1) allows us to compute the total state ρ initially describing all three qubits employed in the teleportation protocol (see Eq. (3)). Using ρ we can evaluate Eq. (9) and insert it along with Eq. (15) into Eq. (20) to obtain the four success rates \overline{Q}_j , each of which is associated with the average probability of measuring the generalized Bell state $|B_j^\varphi\rangle$. Those success rates can be written as follows,

$$\overline{Q}_1 = \overline{Q}_4 = q(\varphi), \quad (25)$$

$$\overline{Q}_2 = \overline{Q}_3 = q(\pi/2 \pm \varphi), \quad (26)$$

where

$$q(\varphi) = \frac{1}{4} - \frac{\cos(2\varphi) [\eta \Delta_h \sinh(\beta\chi) + \chi \Sigma_h e^{2\beta j_z} \sinh(\beta\eta)]}{4\chi\eta [\cosh(\beta\chi) + e^{2\beta j_z} \cosh(\beta\eta)]}. \quad (27)$$

In Eq. (27), $\beta = 1/kT$ and φ were already defined in Eqs. (2) and (4), respectively, while the other quantities are given as follows,

$$\eta = \sqrt{\Delta_j^2 + \Sigma_h^2}, \quad \Delta_j = j_x - j_y, \quad \Sigma_h = h_a + h_b, \quad (28)$$

$$\chi = \sqrt{\Delta_h^2 + \Sigma_j^2}, \quad \Delta_h = h_a - h_b, \quad \Sigma_j = j_x + j_y. \quad (29)$$

We now turn our attention to the efficiency of the teleportation protocol (average fidelities). Before we proceed it is important to recall that the unitary operation U_j that Bob must implement on his qubit at the end of the protocol depends, in addition to Alice's measurement result, on which quantum channel (entangled state) she shares with Bob. In the original protocol [1], for each one of the four possible Bell states (maximally entangled pure states) that Alice and Bob might share, we can associate a set S containing four U_j . Each member of S corresponds to the unitary operation that Bob needs to implement on his qubit according to Alice's measurement result (see Sec. II A).

Here we deal with a mixed state channel which, similarly to any two-qubit state, can be written as $\rho_{ch} = p_{\Phi^+} |\Phi^+\rangle\langle\Phi^+| + p_{\Phi^-} |\Phi^-\rangle\langle\Phi^-| + p_{\Psi^+} |\Psi^+\rangle\langle\Psi^+| + p_{\Psi^-} |\Psi^-\rangle\langle\Psi^-| + \text{non-diagonal terms}$. We are employing the Bell states as a basis to expand ρ_{ch} and thus p_j , $j = \Phi^+, \Phi^-, \Psi^+, \Psi^-$, are the probabilities of projecting ρ_{ch} onto the respective Bell states. Depending on the parameters of Eq. (24), one (or more) p_j dominates and it is expected that the set S associated with the corresponding Bell state will yield the best efficiency for the teleportation protocol. Therefore, in our search for the optimal protocol, we compute the efficiencies of the probabilistic and deterministic protocols, Eqs. (22) and (23), using the four possible sets S . In the end, i.e., after we optimize all expressions with respect to the free parameters of the protocol, we pick out of all possibilities the one giving the greatest efficiency.

1. The deterministic protocol

Let us begin analyzing the efficiency for the deterministic protocol, Eq. (23), where we append a superscript to $\langle\bar{F}\rangle$ to remind us of which set $S = \{U_1, U_2, U_3, U_4\}$ of unitary operations we employ in the calculation of $\langle\bar{F}\rangle$. For example, $\langle\bar{F}\rangle^{\Phi^+}$ means that we use the set S associated to the case where the quantum channel is the Bell state $|\Phi^+\rangle$ (see Sec. II A). Using Eqs. (9), (10), (15), and

(21) in Eq. (23) we get

$$\langle\bar{F}\rangle^{\Phi^+} = f^\Phi(\varphi), \quad (30)$$

$$\langle\bar{F}\rangle^{\Phi^-} = f^\Phi(-\varphi), \quad (31)$$

$$\langle\bar{F}\rangle^{\Psi^+} = f^\Psi(\varphi), \quad (32)$$

$$\langle\bar{F}\rangle^{\Psi^-} = f^\Psi(-\varphi), \quad (33)$$

where

$$f^\Phi(\varphi) = \frac{1}{3} + \frac{\chi \cosh(\beta\chi) - \Sigma_j \sin(2\varphi) \sinh(\beta\chi)}{3\chi [\cosh(\beta\chi) + e^{2\beta j_z} \cosh(\beta\eta)]}, \quad (34)$$

$$f^\Psi(\varphi) = \frac{1}{3} + \frac{\eta \cosh(\beta\eta) - \Delta_j \sin(2\varphi) \sinh(\beta\eta)}{3\eta [e^{-2\beta j_z} \cosh(\beta\chi) + \cosh(\beta\eta)]}. \quad (35)$$

Looking at Eqs. (34) and (35), and noting that β , χ , and η are positive quantities, we easily see that the optimal expressions are obtained by setting $\varphi = \pm\pi/4$. In other words, the measurement basis Alice must employ is the standard Bell basis. More specifically, we must choose φ such that $-\Sigma_j \sin(2\varphi) = |\Sigma_j|$ and $-\Delta_j \sin(2\varphi) = |\Delta_j|$. If $\Sigma_j < 0$ we choose $\varphi = \pi/4$ and when $\Sigma_j > 0$ we set $\varphi = -\pi/4$ (or $5\pi/4$). A similar analysis applies to Δ_j . Therefore, the optimal average fidelities for each set S are

$$\langle\bar{F}\rangle_{opt}^{\Phi^+} = \langle\bar{F}\rangle_{opt}^{\Phi^-} = f_{opt}^\Phi, \quad (36)$$

$$\langle\bar{F}\rangle_{opt}^{\Psi^+} = \langle\bar{F}\rangle_{opt}^{\Psi^-} = f_{opt}^\Psi, \quad (37)$$

where

$$f_{opt}^\Phi = \frac{1}{3} + \frac{\chi \cosh(\beta\chi) + |\Sigma_j| \sinh(\beta\chi)}{3\chi [\cosh(\beta\chi) + e^{2\beta j_z} \cosh(\beta\eta)]}, \quad (38)$$

$$f_{opt}^\Psi = \frac{1}{3} + \frac{\eta \cosh(\beta\eta) + |\Delta_j| \sinh(\beta\eta)}{3\eta [e^{-2\beta j_z} \cosh(\beta\chi) + \cosh(\beta\eta)]}. \quad (39)$$

Finally, the optimal efficiency for the deterministic teleportation protocol is given by

$$\langle\bar{F}\rangle_{opt} = \max\{f_{opt}^\Phi, f_{opt}^\Psi\}. \quad (40)$$

Equation (40) is the benchmark we want to surpass using the probabilistic protocol.

2. The probabilistic protocol

Following the superscript notation just introduced in the preceding analysis, we now need to evaluate \bar{F}_j^ϵ , Eq. (22), for $j = 1, 2, 3, 4$ and $\epsilon = \Phi^+, \Phi^-, \Psi^+, \Psi^-$. Here each j represents one of the four possible measurement outcomes of Alice, i.e., it denotes which generalized Bell state $|B_j^\varphi\rangle$ she measured, and ϵ represents which set of unitary operations S Bob uses to properly correct his qubit, where each element of the set corresponds to a given measurement result of Alice. For instance, $\bar{F}_1^{\Phi^+}$

means that Alice and Bob are working with the postselected measurement outcome $|B_1^\varphi\rangle$, discarding the other three possible measurement results, and Bob's unitary operation for all valid runs of the protocol is always $\mathbb{1}$ (the respective U_1 associated with $\epsilon = \Phi^+$). In Table I we list all 16 possibilities.

TABLE I: In the table below we list to each \overline{F}_j^ϵ the corresponding Alice's measurement outcome $|B_j^\varphi\rangle$ and the respective unitary operation Bob implements on his qubit.

$\overline{F}_1^{\Phi^+} \rightarrow B_1^\varphi\rangle \rightarrow \mathbb{1}$	$\overline{F}_1^{\Phi^-} \rightarrow B_1^\varphi\rangle \rightarrow \sigma_z$
$\overline{F}_2^{\Phi^+} \rightarrow B_2^\varphi\rangle \rightarrow \sigma_z$	$\overline{F}_2^{\Phi^-} \rightarrow B_2^\varphi\rangle \rightarrow \mathbb{1}$
$\overline{F}_3^{\Phi^+} \rightarrow B_3^\varphi\rangle \rightarrow \sigma_x$	$\overline{F}_3^{\Phi^-} \rightarrow B_3^\varphi\rangle \rightarrow \sigma_z \sigma_x$
$\overline{F}_4^{\Phi^+} \rightarrow B_4^\varphi\rangle \rightarrow \sigma_z \sigma_x$	$\overline{F}_4^{\Phi^-} \rightarrow B_4^\varphi\rangle \rightarrow \sigma_x$
$\overline{F}_1^{\Psi^+} \rightarrow B_1^\varphi\rangle \rightarrow \sigma_x$	$\overline{F}_1^{\Psi^-} \rightarrow B_1^\varphi\rangle \rightarrow \sigma_z \sigma_x$
$\overline{F}_2^{\Psi^+} \rightarrow B_2^\varphi\rangle \rightarrow \sigma_z \sigma_x$	$\overline{F}_2^{\Psi^-} \rightarrow B_2^\varphi\rangle \rightarrow \sigma_x$
$\overline{F}_3^{\Psi^+} \rightarrow B_3^\varphi\rangle \rightarrow \mathbb{1}$	$\overline{F}_3^{\Psi^-} \rightarrow B_3^\varphi\rangle \rightarrow \sigma_z$
$\overline{F}_4^{\Psi^+} \rightarrow B_4^\varphi\rangle \rightarrow \sigma_z$	$\overline{F}_4^{\Psi^-} \rightarrow B_4^\varphi\rangle \rightarrow \mathbb{1}$

Inserting Eqs. (9), (15), and (21) into (22), and using the proper unitary operation U_j (see Table I) to compute ρ_{B_j} , Eq. (10), we get

$$\overline{F}_1^{\Phi^+} = \overline{F}_4^{\Phi^+} = g^\Phi(\varphi), \quad (41)$$

$$\overline{F}_2^{\Phi^+} = \overline{F}_3^{\Phi^+} = g^\Phi(\pi/2 - \varphi), \quad (42)$$

$$\overline{F}_1^{\Phi^-} = \overline{F}_4^{\Phi^-} = g^\Phi(-\varphi), \quad (43)$$

$$\overline{F}_2^{\Phi^-} = \overline{F}_3^{\Phi^-} = g^\Phi(\pi/2 + \varphi), \quad (44)$$

$$\overline{F}_1^{\Psi^+} = \overline{F}_4^{\Psi^+} = g^\Psi(\varphi), \quad (45)$$

$$\overline{F}_2^{\Psi^+} = \overline{F}_3^{\Psi^+} = g^\Psi(\pi/2 - \varphi), \quad (46)$$

$$\overline{F}_1^{\Psi^-} = \overline{F}_4^{\Psi^-} = g^\Psi(-\varphi), \quad (47)$$

$$\overline{F}_2^{\Psi^-} = \overline{F}_3^{\Psi^-} = g^\Psi(\pi/2 + \varphi), \quad (48)$$

where

$$g^\Phi(\varphi) = \frac{1}{3} + \frac{\eta\{\chi \cosh(\beta\chi) - \sinh(\beta\chi)[\Delta_h \cos(2\varphi) + \Sigma_j \sin(2\varphi)]\}}{3\{\eta\chi[\cosh(\beta\chi) + e^{2\beta j_z} \cosh(\beta\eta)] - \cos(2\varphi)[\eta\Delta_h \sinh(\beta\chi) + \chi\Sigma_h e^{2\beta j_z} \sinh(\beta\eta)]\}}, \quad (49)$$

$$g^\Psi(\varphi) = \frac{1}{3} + \frac{\chi\{\eta \cosh(\beta\eta) - \sinh(\beta\eta)[\Delta_j \sin(2\varphi) + \Sigma_h \cos(2\varphi)]\}}{3\{\eta\chi[e^{-2\beta j_z} \cosh(\beta\chi) + \cosh(\beta\eta)] - \cos(2\varphi)[\eta\Delta_h e^{-2\beta j_z} \sinh(\beta\chi) + \chi\Sigma_h \sinh(\beta\eta)]\}}. \quad (50)$$

The first important thing worth noting if we look at Eqs. (49) and (50) is the fact that $\varphi = \pm\pi/4$ (or $\varphi = \pm 3\pi/4$) are not in general the optimal settings. In other words, the optimal measurement basis are not formed by the standard maximally entangled Bell states. Indeed, whenever an external magnetic field is present, either Δ_h or Σ_h (or both) is not zero. This leads to the presence of the $\cos(2\varphi)$ terms, in addition to the $\sin(2\varphi)$ terms, in Eqs. (49) and (50). The optimal φ in this case can be found by solving the equations $dg^\epsilon/d\varphi = 0$, $\epsilon = \Phi, \Psi$, and then selecting the g^ϵ giving the greatest efficiency.

Second, comparing Eqs. (49) and (50) with (34) and (35), it is not difficult to see that

$$g^\epsilon(\varphi) = f^\epsilon(\varphi), \text{ if } \Delta_h = \Sigma_h = 0. \quad (51)$$

This means that if we have no external fields ($\Delta_h = \Sigma_h = 0$), the probabilistic teleportation protocol gives exactly the same efficiencies of the deterministic protocol. We thus arrive at the important conclusion that the probabilistic protocol can only beat the deterministic one if external magnetic fields are turned on.

There is another interesting feature of the present probabilistic protocol. Looking at Eqs. (41)-(48) we see that we always have $\overline{F}_1^\epsilon = \overline{F}_4^\epsilon$ and $\overline{F}_2^\epsilon = \overline{F}_3^\epsilon$, which implies that \overline{F}_1^ϵ and \overline{F}_4^ϵ , and equivalently \overline{F}_2^ϵ and \overline{F}_3^ϵ , share the same optimal φ . This property enhances the effective success rate of the probabilistic protocol since two out of

four possible measurement results of Alice give the same optimal efficiency with the same optimal settings. Thus, instead of postselecting only one outcome, Alice and Bob can postselect two measurement outcomes, increasing the success rate to twice the value given in Eq. (27),

$$\overline{Q}_{1,4} = 2q(\varphi), \quad (52)$$

$$\overline{Q}_{2,3} = 2q(\varphi \pm \pi/2). \quad (53)$$

Finally, putting together all the pieces of information in the last paragraphs, and noting that in Eqs. (49) and (50) the arguments of all sines and cosines are given by 2φ , we can obtain the optimal efficiency for the probabilistic protocol by solving the following maximization problem,

$$\overline{F}_{opt} = \max_{\varphi \in [0, \pi]} \{g^\Phi(\varphi), g^\Psi(\varphi)\}. \quad (54)$$

By ranging φ from 0 to π we can obtain the optimal settings for all instances listed in Eqs. (41)-(48), and by choosing the greatest value from $g^\Phi(\varphi_{opt})$ and $g^\Psi(\varphi_{opt})$, we get the optimal efficiency \overline{F}_{opt} . The corresponding success rate is given by either $2q(\varphi_{opt})$ or $2q(\tilde{\varphi}_{opt})$, where φ_{opt} and $\tilde{\varphi}_{opt}$ are the φ 's maximizing g^Φ and g^Ψ , respectively.

III. RESULTS

We are now ready to study the efficiency to teleport an arbitrary pure state qubit for several quantum channels described by Heisenberg-like models in thermal equilibrium with a heat reservoir at temperature T . We divide our quantum channels into two main groups, all of which subjected to external magnetic fields in the z direction. The first group encompasses all models in which there is no $\sigma_z^{(2)}\sigma_z^{(3)}$ interaction and the second one those models possessing it. Note that whenever there is no external fields, the deterministic and probabilistic protocols yield the same results and, thus, we work only with cases in which the external field is present.

A. XY-like models

The one-dimensional XY model in a transverse field is obtained from Eq. (24) by setting $j_z = 0$ and $h_a = h_b$. It is more usual, however, to rewrite Eq. (24) as follows [32],

$$H = -\lambda[(1 + \zeta)\sigma_x^{(2)}\sigma_x^{(3)} + (1 - \zeta)\sigma_y^{(2)}\sigma_y^{(3)}] - \sigma_z^{(2)} - \sigma_z^{(3)}, \quad (55)$$

with $\lambda \geq 0$ being the inverse of the magnitude of the external field and ζ the anisotropy parameter. The Ising model is obtained when $\zeta = \pm 1$ and for $\zeta = 0$ we get the XX model in a transverse field. At $T = 0$ and in the thermodynamic limit (infinite chain), the XY model has a quantum critical point at $\lambda = 1$, where a second-order quantum phase transition separates a ferromagnetic ordered phase from a paramagnetic one [38–41].

1. Efficiency as a function of T

We first analyze the optimal efficiencies (average fidelities) of the deterministic and probabilistic protocols, Eqs. (40) and (54) respectively, as a function of the temperature T . We start with the Ising model in a transverse field, whose main results are shown in Fig. 2.

Looking at Fig. 2 we note that the efficiency is a monotonically decreasing function of the temperature and that for $kT \approx 1.2$ the optimal efficiencies for the deterministic and probabilistic protocols are almost the same. As we continue to increase the temperature, we arrive at a value of T after which the efficiency of the protocol is below $2/3$. This value for the average fidelity is called the classical limit since any protocol with average fidelities lower than $2/3$ can be implemented without Alice and Bob sharing an entangled quantum channel [47].

For low values of T , however, we can have considerable gains in efficiency by working with the probabilistic protocol. For instance, whenever $kT < 0.2$, the probabilistic protocol yields an almost perfect teleportation, a considerable improvement over the deterministic one. In this case the success rate is about 10% when $\lambda = 0.7$ and 30%

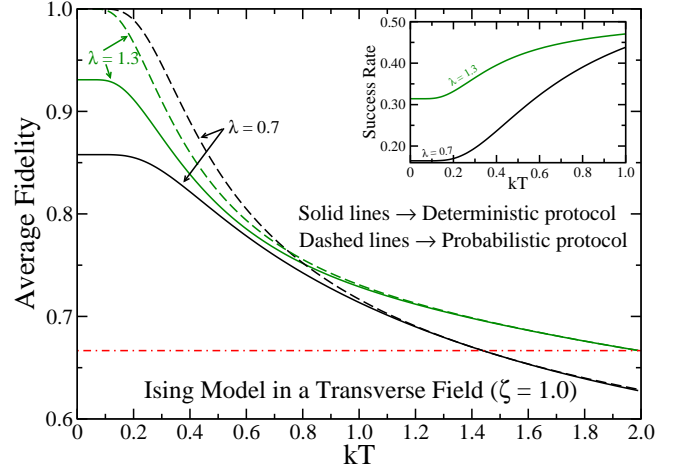


FIG. 2: (color online) Main plot: The efficiencies for the deterministic (solid curves) and probabilistic (dashed curves) teleportation protocols as a function of the temperature when the quantum channel connecting Alice and Bob is given by the thermalized Ising model in a transverse field. The efficiency for the deterministic protocol is given by Eq. (40) and for the probabilistic one by Eq. (54). The dotted-dashed red line marks the classical limit ($2/3$) below which the teleportation protocol can be matched by a purely classical protocol. Inset: The success rate (probability of success) for the probabilistic protocol. Here and in the following figures all quantities are dimensionless.

when $\lambda = 1.3$. We also note that the optimal efficiencies for the deterministic and probabilistic protocols are given by f_{opt}^p and $g^p(\varphi)$, respectively (see Eqs. (40) and (54)). Moreover, the optimal φ for the latter depends on T and is not equal to $\pm\pi/4$.

Moving to the XX and XY models, i.e., turning on the $\sigma_y^{(2)}\sigma_y^{(3)}$ interaction, we observe the following two similar and interesting trends (see Figs. 3 and 4). First, whenever $\lambda < 1$ (ferromagnetic phase) there exists a range of values of temperature where the efficiency of the probabilistic protocol *increases* with T . This is a remarkable property and tells us that working with a “warmer” quantum channel is better than working with a “colder” one. We can understand this behavior noting that under certain configurations of the coupling constants, the ground state of the Hamiltonian has little or no entanglement at all, although the first excited states are highly entangled ones and very close to Bell states [26]. Thus, by increasing the temperature we start to populate those highly entangled states in such a manner that a warmer quantum channel has more entanglement than a colder one. The latter effect is more intense in the probabilistic protocol where, by postselecting the appropriate measurement results, we may project the quantum channel ρ_{ch} onto highly entangled states and consequently enhance even more the efficiency of the teleportation protocol. If we continue to increase the temperature, however, more and more states get populated and we start to get a less entangled channel, reducing the efficiency of the protocol.

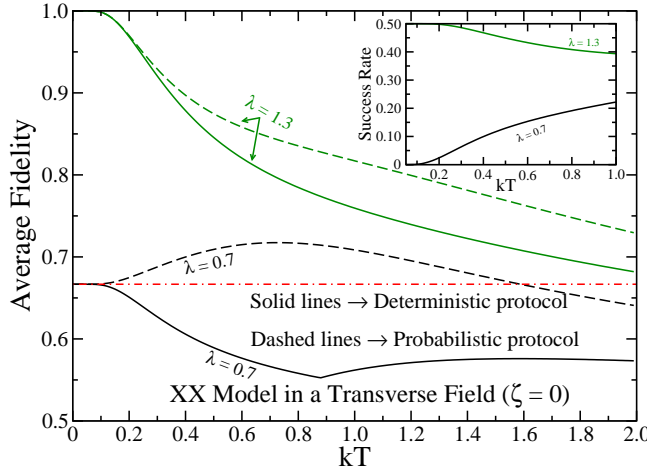


FIG. 3: (color online) Same as Fig. 2 but now we work with the isotropic XX model in a transverse field. Note that under certain conditions ($\lambda < 1$) the efficiency for the probabilistic protocol may increase with the temperature and be the only one yielding an efficiency greater than the classical threshold (2/3). Also, the optimal φ for the probabilistic protocol depends on T and is not equal to $\pm\pi/4$, with the latter being the optimal settings for the deterministic case.

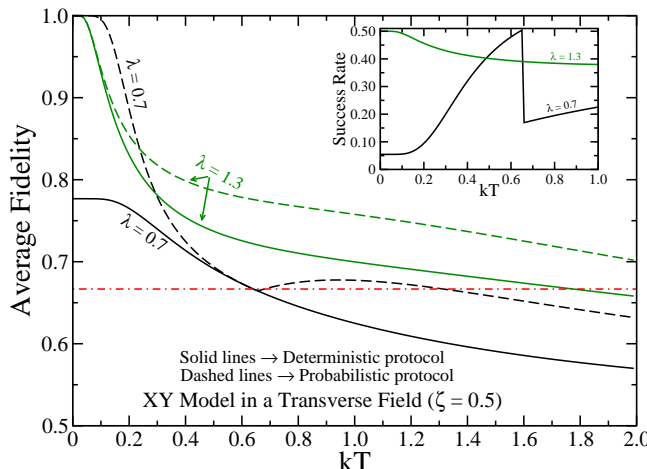


FIG. 4: (color online) Same as Figs. 2 and 3 but now we have the anisotropic XY model in a transverse field.

For sufficiently high temperatures the quantum channel is nearly described by a completely mixed state with no entanglement at all. This is why we always end up with efficiencies lower than 2/3 for very high temperatures.

Second, another important characteristic shared by the XX and XY models is the fact that for certain values of T the efficiency for the deterministic protocol does not surpass the classical limit 2/3, while the probabilistic protocol's efficiency does. In this scenario, therefore, we can only get a truly quantum teleportation if we employ the probabilistic protocol.

There are also different characteristics between the XX and XY models. For example, the deterministic proto-

col for the XX model does not yield an average fidelity greater than the classical limit for $\lambda < 1$. This is only possible when we use the probabilistic protocol. For the XY model, however, there is no such restriction and we can have for $\lambda < 1$ the average fidelity for both the deterministic and probabilistic protocols greater than 2/3 if we work at a sufficiently low temperature.

Another distinctive feature of the XX model is the fact that whenever the optimal average fidelities for the deterministic and probabilistic protocols are greater than 2/3, f_{opt}^p and $g^p(\varphi)$, respectively, are the functions optimizing the efficiency (see Eqs. (40) and (54)). For the XY model, however, the functions leading to the optimal efficiency for certain values of T may be different for the probabilistic protocol when the efficiency is greater than 2/3. In this case either $g^p(\varphi)$ or $g^v(\varphi)$ may give the optimal efficiency. This is the reason for the cusp of the curve of the optimal average fidelity (the $\lambda = 0.7$ dashed curve) and for the discontinuity in the success rate (the $\lambda = 0.7$ curve in the inset) that we see for the probabilistic protocol in Fig. 4. The cusp for the efficiency curve and the discontinuity for the probability of success curve occur exactly at the temperature in which $g^p(\varphi)$ and $g^v(\varphi)$ exchange roles. Below this temperature $g^p(\varphi)$ gives the optimal efficiency while above it $g^v(\varphi)$ does.

2. Efficiency as a function of the external field

We now turn our attention to the behavior of the average fidelities for the deterministic and probabilistic protocols as functions of the inverse of the strength of the external magnetic field λ . Starting with the Ising model in a transverse field (upper panel of Fig. 5), we note that for a fixed temperature there is an optimal λ that gives the greatest efficiency and that the optimal λ 's are different for the deterministic and probabilistic protocols. This is most clearly seen looking at the curves for $kT = 0.3$. We also see that the probabilistic protocol outperforms by far the deterministic one for small values of λ .

Studying the XX model (left lower panel of Fig. 5), we note that the greater the value of λ the better the efficiency of the probabilistic protocol. For the deterministic protocol, an increase of λ increases the efficiency only for λ greater than a certain critical value that depends on T . Also, when $\lambda < 1$ the average fidelity for the deterministic protocol does not exceed 2/3. It is interesting to note that the efficiencies for the probabilistic protocols, and in particular for the deterministic ones, change abruptly near the quantum critical point $\lambda = 1$.

Near the quantum critical point $\lambda = 1$ there is a similar abrupt behavior for the efficiencies of the deterministic and probabilistic protocols for the XY model (right lower panel of Fig. 5). In this case the average fidelities tend to their minimum values near the critical point. As we move to the right or left of the critical point the efficiency starts to increase. For $\lambda > 1$ this trend continues as we increase λ while for $\lambda < 1$ the average fidelity starts to decrease

after reaching a local maximum. This behavior is clearer the greater the value of T . Finally, the reason for the cusps in the curves for the efficiencies is again related to which of the functions f_{opt}^p or f_{opt}^v ($g^p(\varphi)$ or $g^v(\varphi)$) gives the optimal average fidelity for the deterministic (probabilistic) protocol. For small λ , f_{opt}^p and $g^p(\varphi)$ give the highest efficiencies and, as we increase λ , f_{opt}^v and $g^v(\varphi)$ dominate after we cross a certain value of λ that depends on T .

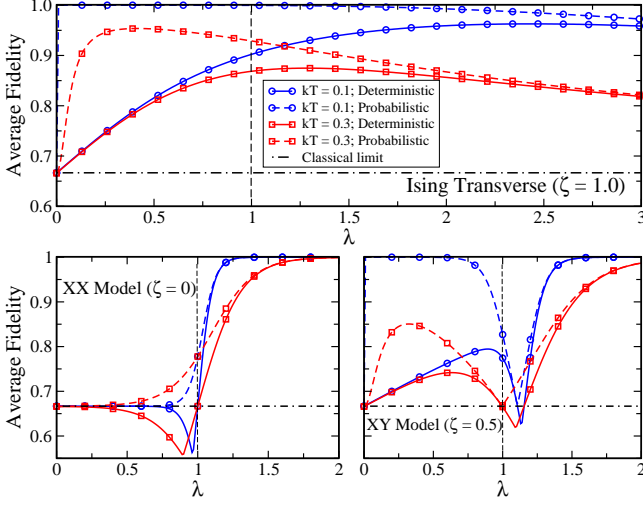


FIG. 5: (color online) The optimal efficiencies of the deterministic (solid curves) and probabilistic (dashed curves) teleportation protocols as a function of λ for the Ising model (upper panel), the XX model (left lower panel), and the XY model (right lower panel), all of them in an external magnetic field of strength $1/\lambda$. Circles denote $kT = 0.1$ and squares $kT = 0.3$. The dotted-dashed black lines delimit the classical limit $2/3$.

B. XXZ-like models

The one-dimensional XXZ model in an external field in the z direction is obtained from Eq. (24) when we set $j_x = j_y$ and $h_a = h_b$. This model is usually written as [32]

$$H = 2J[\sigma_x^{(2)}\sigma_x^{(3)} + \sigma_y^{(2)}\sigma_y^{(3)} + \Delta\sigma_z^{(2)}\sigma_z^{(3)}] - \frac{h}{2}[\sigma_z^{(2)} + \sigma_z^{(3)}], \quad (56)$$

where J is the exchange constant, Δ the anisotropy parameter, and h the external field. When $\Delta = 1$ we have the isotropic XXX model and for $\Delta \neq 0$ we get the anisotropic XXZ model. In the thermodynamic limit and at $T = 0$ the XXZ model has two quantum critical points [42–46]: Δ_{inf} , where an infinite order quantum phase transition takes place, and Δ_1 , where a first-order quantum phase transition happens. The expressions giving those critical points are not so simple and can be found in Refs. [42, 43].

1. Efficiency as a function of T

Let us start studying the isotropic XXX model ($\Delta = 1$). The first thing worth noting is that for $J < 0$ the efficiencies for both the deterministic and probabilistic protocols do not surpass the classical limit $2/3$, even for low T . We thus restrict the following analysis to the cases in which $J > 0$. It can also be proved that for the deterministic protocol $f_{opt}^p \leq 2/3$ and thus, since we are interested in the cases surpassing the classical limit, instead of Eq. (40) we work only with f_{opt}^v in the determination of the optimal efficiency. The curves for the deterministic protocol in Figs. 6 and 8 show f_{opt}^v . Also, by setting the magnetic field to $h = 8.0$ we get that the first-order quantum phase transition for this model occurs at $J_c = 1.0$.

Looking at Fig. 6 we note that we have two regimes for the behavior of the average fidelities. For $J < J_c$ the deterministic protocol does not give an efficiency greater than $2/3$. In this regime the classical limit can only be surpassed using the probabilistic protocol. Indeed, for $kT \lesssim 5.0$ the probabilistic protocol yields an efficiency greater than $2/3$ and greater than that of the deterministic protocol, with success rates of the order of 10%. We also see that in this range of temperatures there are instances where the efficiency *increases* with T .

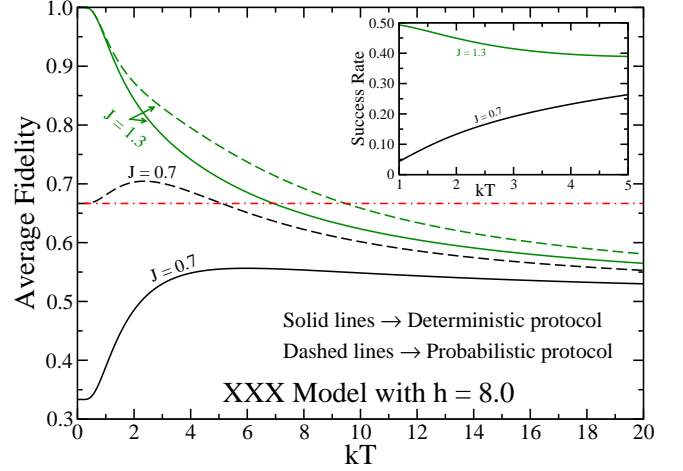


FIG. 6: (color online) Main plot: The average fidelities (efficiencies) of the deterministic (solid curves) and probabilistic (dashed curves) teleportation protocols as a function of the temperature when the quantum channel connecting Alice and Bob is the thermalized XXX model in an external field. As explained in the text, for the deterministic protocol we plot f_{opt}^v and for the probabilistic one Eq. (54). The dotted-dashed red line marks the classical limit ($2/3$) below which the teleportation protocol can be matched by a purely classical protocol. Inset: The success rate (probability of success) for the probabilistic protocol.

For $J > J_c$, on the other hand, both the deterministic and probabilistic protocols can yield efficiencies above the classical limit. In this regime the efficiencies are always a monotonically decreasing function of the temperature

and we still have a small range of temperatures in which only the probabilistic protocol gives an average fidelity greater than $2/3$. For all values of $J > 0$ the optimal efficiency for the probabilistic protocol is given by $g^*(\varphi)$, with the optimal φ being different from $\pm\pi/4$ and dependent on T .

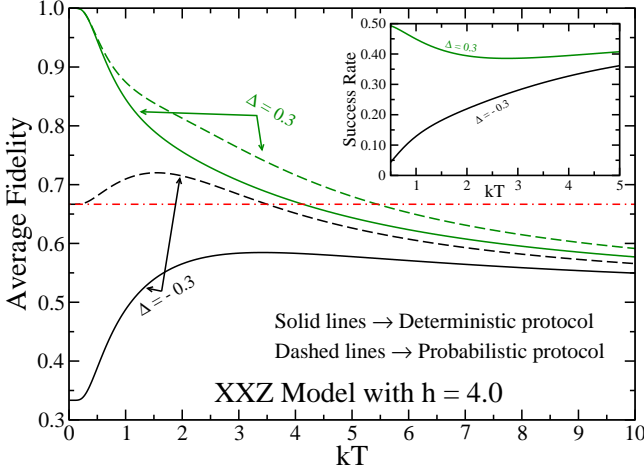


FIG. 7: (color online) Same as Fig. 6 but now we work with the XXZ model with an external field in the z direction.

We now focus our attention at the XXZ model in an external field in the z direction. We set $J = 1.0$ and the magnitude of the field ($h = 4.0$) such that the first-order quantum phase transition occurs at $\Delta_1 = 0$. Here we can also prove that $f_{opt}^p \leq 2/3$ for the deterministic protocol and similarly to the XXX model, we show f_{opt}^v instead of Eq. (40) in Figs. 7 and 8 when analyzing the deterministic protocol.

Looking at Fig. 7 we note that many features seen for the XXX model are also present in the XXZ model. Indeed, we have two regimes for the behavior of the efficiency of the protocol. One before ($\Delta < \Delta_1$) and another after ($\Delta > \Delta_1$) the quantum critical point delimiting the first-order quantum phase transition. For $\Delta < \Delta_1$ only the probabilistic protocol yields average fidelities greater than the classical limit, with success rates lying between 10% to 20% for a considerable set of values of $\Delta < \Delta_1$. We also have ranges of temperatures where the efficiency of the probabilistic protocol *increases* with T .

For $\Delta > \Delta_1$ the efficiencies are monotonically decreasing functions of T and both the deterministic and probabilistic protocols can work above the classical limit at sufficiently low temperatures. We also have small ranges of T in which the probabilistic protocol leads to an efficiency greater than $2/3$ while the deterministic protocol works below this value.

Finally, and similarly to the XXX model, whenever the efficiency is above the classical limit, the functions leading to the optimal efficiencies are f_{opt}^v for the deterministic and $g^*(\varphi)$ for the probabilistic protocols. The optimal values of φ for the probabilistic protocol depend on T and are not $\pm\pi/4$, the optimal ones for the deter-

ministic case.

2. Efficiency as a function of the coupling constants

We now investigate how the efficiencies (average fidelities) for the deterministic and probabilistic protocols behave as a function of the exchange constant J for the XXX model and of the anisotropy parameter Δ for the XXZ model.

For the XXX model we keep as before $h = 8.0$ and for several values of kT we compute the efficiency as a function of J (upper panel of Fig. 8), including values of J near and at the critical point $J_c = 1.0$. For the XXZ model we set $h = 4.0$ and $J = 1.0$, which leads to a critical point $\Delta_1 = 0$, and we also evaluate for several values of kT the efficiency as a function of Δ (lower panel of Fig. 8), including values of Δ near and at the critical point Δ_1 .

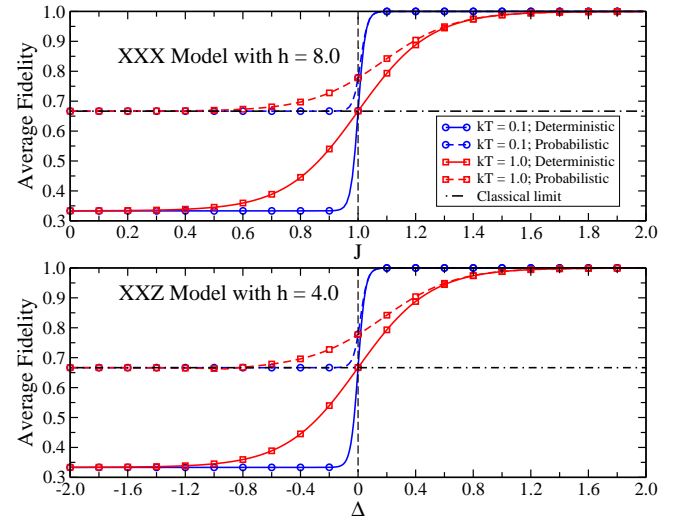


FIG. 8: (color online) The optimal efficiencies of the deterministic (solid curves) and probabilistic (dashed curves) teleportation protocols as a function of J for the XXX model (upper panel) and of Δ for the XXZ model (lower panel). As discussed in the text, for the deterministic protocol we plot f_{opt}^v and for the probabilistic one Eq. (54). Circles denote $kT = 0.1$ and squares $kT = 1.0$. The dotted-dashed black lines delimit the classical limit $2/3$.

Looking at Fig. 8 we note that the efficiencies for the XXX and XXZ models, as functions of J and Δ , respectively, share the same qualitative features. In particular, we note a clear distinctive behavior for the optimal average fidelities before and after the first-order quantum critical points, even at considerably high temperatures ($kT \approx 1.0$). It is now clear that below the critical point the deterministic protocols do not yield an efficiency greater than the classical limit $2/3$ while the probabilistic protocols do. We also observe that for sufficiently high values of J and Δ , above the critical points, the efficiencies for the deterministic and probabilistic pro-

ocols converge to their greatest possible value, leading to a perfect teleportation. Moreover, at low values of J or Δ , the functions f_{opt}^{Φ} and $g^{\Phi}(\varphi)$ give the optimal average fidelities. As we approach the critical point, f_{opt}^{Ψ} and $g^{\Psi}(\varphi)$ dominate and furnish the optimal values for the efficiencies. Note that this exchange of functions leading to the optimal efficiencies never occurs exactly at the critical point for finite T .

It is also worth noting that we have computed the efficiencies about and at the other quantum critical point, where an infinite-order quantum phase transition happens (Δ_{inf}). For the present XXZ model with $h = 4.0$ and $J = 1.0$ we obtain $\Delta_{inf} \approx 2.74$ [31, 42, 43]. We have not observed, however, any quantitative or qualitative changes in the behavior of the efficiencies. Actually, before reaching Δ_{inf} the efficiency of the teleportation protocol already saturates to its highest possible value and no changes are seen after that value is attained.

IV. CONCLUSION

We have extensively studied the probabilistic teleportation protocol when the quantum channel connecting Alice and Bob is given by interacting two-qubit systems in equilibrium with a thermal reservoir. In this scenario the quantum state describing the quantum channel is the canonical ensemble density matrix and any entanglement present in that state is usually dubbed *thermal entanglement* [24–32].

We worked with several standard Heisenberg-like models in order to describe the interaction between the two qubits of the quantum channel. Those models are widely employed to describe the interaction between two or more spins in several condensed matter systems and can be used to describe the interactions we might face when building a quantum computer or a quantum communication protocol operating on solid state devices. Being more specific, we studied the Ising model, the XX model, the XY model, the isotropic XXX model, and the anisotropic XXZ model. We also considered the cases where an external magnetic field is applied in the z direction.

After studying all those models three important common features emerged. First, we proved analytically that the efficiency for the probabilistic protocol can only be greater than the efficiency of the deterministic protocol if we have an external magnetic field. Whenever the external field is zero, the probabilistic and deterministic protocols have exactly the same efficiency.

Second, whenever the probabilistic teleportation protocol outperforms the deterministic protocol, the measurement basis employed by Alice during the execution of the teleportation protocol is not the standard Bell basis, which is spanned by four maximally entangled states. The optimal measurement basis for the probabilistic protocol is given by the generalized Bell states, whose entanglement degree is not maximal. Moreover, the appropri-

ate generalized Bell basis depends on the value of the temperature and on which Heisenberg-like model we are working with.

Third, the optimal settings leading to the optimal efficiency for the probabilistic protocol are the same for two out of four possible measurement results that Alice may obtain at each run of the protocol. Thus, the success rate for the probabilistic protocol is enhanced since Alice and Bob can postselect two instead of one measurement result at each run of the protocol. In general, the success rate for the probabilistic protocols here studied are above 10%, being much higher than this value under certain arrangements.

Other three features are clearly shared by all models here investigated with the exception of the Ising model. The first one is related to the fact that *more* heat (higher temperatures) may lead to a *more* efficient probabilistic teleportation. In the notation of the present paper, this happens whenever the coupling constants and the external magnetic field are such that the system lies below the quantum critical point separating its two phases. In the appropriate phase, there exists a scenario in which the efficiency increases with increasing temperature.

Another characteristic shared by almost all models is the fact that under the same conditions the optimal efficiencies for the probabilistic and deterministic protocols may differ in a very important way. There are ranges of temperatures where only the probabilistic protocol crosses the classical limit of $2/3$ for the optimal average fidelity. Below this value any teleportation protocol can be simulated by a “classical” protocol, where no entanglement at all is needed between Alice and Bob. Only local operations and classical communication (LOCC) suffice to deliver the same efficiency. Thus, whenever this happens, we can only have a truly quantum teleportation if we work with the probabilistic protocol. The deterministic protocol fails in delivering a quantum teleportation that is genuinely quantum.

Third, we have also noted that the behavior for the efficiencies of the deterministic and probabilistic protocols may be qualitatively and quantitatively affected in the vicinity of the quantum critical points, even at finite temperatures. For instance, for the XX, XXX and XXZ models the optimal efficiencies can only surpass the classical limit $2/3$ as we approach the critical point from below. The lower the temperature the more the quantum critical point marks this transition in the behavior for the efficiency. For the XX and XY models, we also noted that near the critical point we have the global minimum for the efficiency.

Finally, and similarly to the results of Ref. [23], we have a trade-off between the success rates and the efficiencies for the probabilistic protocols. The optimizations performed here were carried out to maximize the average fidelity without imposing any other restriction. It is possible, however, to increase the success rate by diminishing the efficiency.

Acknowledgments

RF thanks CAPES (Brazilian Agency for the Improvement of Personnel of Higher Education) for funding and GR thanks the Brazilian agencies CNPq (National Council

for Scientific and Technological Development) and CNPq/FAPESP (State of São Paulo Research Foundation) for financial support through the National Institute of Science and Technology for Quantum Information.

[1] C. H. Bennett, G. Brassard, C. Crepeau, R. Jozsa, A. Peres, and W.K. Wootters, *Phys. Rev. Lett.* **70**, 1895 (1993).

[2] L. Vaidman, *Phys. Rev. A* **49**, 1473 (1994).

[3] S. L. Braunstein and H. J. Kimble, *Phys. Rev. Lett.* **80**, 869 (1998).

[4] D. Bouwmeester *et al.*, *Nature (London)* **390**, 575 (1997).

[5] D. Boschi *et al.*, *Phys. Rev. Lett.* **80**, 1121 (1998).

[6] A. Furusawa *et al.*, *Science* **282**, 706 (1998).

[7] C. H. Bennett, G. Brassard, S. Popescu, B. Schumacher, J. A. Smolin, and W. K. Wootters, *Phys. Rev. Lett.* **76**, 722 (1996).

[8] W.-Li Li, C.-Feng Li, and G.-C. Guo, *Phys. Rev. A* **61**, 034301 (2000).

[9] P. Agrawal and A. K. Pati, *Phys. Lett. A* **305**, 12 (2002).

[10] G. Gordon and G. Rigolin, *Phys. Rev. A* **73**, 042309 (2006); G. Gordon and G. Rigolin, *Phys. Rev. A* **73**, 062316 (2006); G. Gordon and G. Rigolin, *Eur. Phys. J. D* **45**, 347 (2007); G. Rigolin, *J. Phys. B: At. Mol. Opt. Phys.* **42**, 235504 (2009); G. Gordon and G. Rigolin, *Opt. Commun.* **283**, 184 (2010); R. Fortes and G. Rigolin, *Ann. Phys. (N.Y.)* **336**, 517 (2013).

[11] G. Bowen and S. Bose, *Phys. Rev. Lett.* **87**, 267901 (2001).

[12] S. Albeverio, S.-M. Fei, and W.-L. Yang, *Phys. Rev. A* **66**, 012301 (2002).

[13] S. Oh, S. Lee, and H.-w Lee, *Phys. Rev. A* **66**, 022316 (2002).

[14] B. G. Taketani, F. de Melo, and R. L. de Matos Filho, *Phys. Rev. A* **85**, 020301(R) (2012).

[15] P. Badziąg, M. Horodecki, P. Horodecki, and R. Horodecki, *Phys. Rev. A* **62**, 012311 (2000).

[16] S. Bandyopadhyay, *Phys. Rev. A* **65**, 022302 (2002).

[17] Y. Yeo, *Phys. Rev. A* **78**, 022334 (2008).

[18] S. Bandyopadhyay and A. Ghosh, *Phys. Rev. A* **86**, 020304(R) (2012).

[19] L. T. Knoll, Ch. T. Schmiegelow, and M. A. Larotonda, *Phys. Rev. A* **90**, 042332 (2014).

[20] R. Fortes and G. Rigolin, *Phys. Rev. A* **92**, 012338 (2015).

[21] F. S. Luiz and G. Rigolin, *Ann. Phys. (N.Y.)* **354**, 409 (2015).

[22] M. M. Cunha, E. A. Fonseca, and F. Parisio, e-print arXiv:1611.01167 [quant-ph].

[23] R. Fortes and G. Rigolin, *Phys. Rev. A* **93**, 062330 (2016).

[24] M. C. Arnesen, S. Bose, and V. Vedral, *Phys. Rev. Lett.* **87**, 017901 (2001).

[25] G. L. Kamta and A. F. Starace, *Phys. Rev. Lett.* **88**, 107901 (2002); X. Wang, *Phys. Rev. A* **64**, 012313 (2001); Y. Sun, Y. Chen, and H. Chen, *Phys. Rev. A* **68**, 044301 (2003); S.-J. Gu, H.-Q. Lin, and Y.-Q. Li, *Phys. Rev. A* **68**, 042330 (2003).

[26] G. Rigolin, *Int. J. Quant. Inf.* **2**, 393 (2004).

[27] L. Amico and D. Patané, *Europhys. Lett.* **77**, 17001 (2007).

[28] L. Amico *et al.*, *Rev. Mod. Phys.* **80**, 517 (2008); L. Amico and R. Fazio, *J. Phys. A: Math. Theor.* **42**, 504001 (2009).

[29] T. Werlang and G. Rigolin, *Phys. Rev. A* **81**, 044101 (2010).

[30] T. Werlang, C. Trippe, G.A.P. Ribeiro, and G. Rigolin, *Phys. Rev. Lett.* **105**, 095702 (2010).

[31] T. Werlang, G.A.P. Ribeiro, and G. Rigolin, *Phys. Rev. A* **83**, 062334 (2011).

[32] T. Werlang, G.A.P. Ribeiro, and G. Rigolin, *Int. J. Mod. Phys. B* **27**, 1345032 (2013).

[33] W.K. Wootters, *Phys. Rev. Lett.* **80**, 2245 (1998).

[34] K. Kraus, *States, Effects and Operations: Fundamental Notions of Quantum Theory* (Springer-Verlag, Berlin, 1983).

[35] M. A. Nielsen and I. L. Chuang, *Quantum Computation and Quantum Information* (Cambridge University Press, Cambridge, 2000).

[36] A. Uhlmann, *Rep. Math. Phys.* **9**, 273 (1976).

[37] S. Massar and S. Popescu, *Phys. Rev. Lett.* **74**, 1259 (1995); S. L. Braunstein, Ch. A. Fuchs, and H. J. Kimble, *J. Mod. Opt.* **47**, 267 (2000); H. Barnum, PhD thesis (University of New Mexico, Albuquerque, 1998).

[38] E. Lieb, T. Schultz and D. Mattis, *Ann. Phys.* **16**, 407 (1961).

[39] E. Barouch, B. M. McCoy and M. Dresden, *Phys. Rev. A* **2**, 1075 (1970).

[40] E. Barouch and B. M. McCoy, *Phys. Rev. A* **3**, 786 (1971).

[41] P. Pfeuty, *Ann. Phys. (New York)* **57**, 79 (1970).

[42] J. Cloizeaux and M. Gaudin, *J. Math. Phys.* **7**, 1384 (1966).

[43] M. Takahashi, *Thermodynamics of One-Dimensional Solvable Models* (Cambridge University Press, Cambridge, England, 1999).

[44] M. Bortz and F. Göhmann, *Eur. Phys. J. B* **46**, 399 (2005).

[45] H. E. Boos *et al.*, *J. Stat. Mech.* P08010 (2008).

[46] C. Trippe, F. Göhmann and A. Klümper, *Eur. Phys. J. B* **73**, 253 (2010).

[47] S. Massar and S. Popescu, *Phys. Rev. Lett.* **74**, 1259 (1995); S. L. Braunstein, Ch. A. Fuchs, and H. J. Kimble, *J. Mod. Opt.* **47**, 267 (2000); H. Barnum, PhD thesis, University of New Mexico, Albuquerque, NM, 1998.